

# Study on the Mechanical Properties and Failure Characteristics of Reinforced Segments Based on DIC

Xiao Li <sup>1</sup>, Ou Geng <sup>2,\*</sup> and Qian Sun <sup>3</sup>

<sup>1</sup> China Railway Shanghai Design Institute Group Co., Ltd., Xuzhou 221000, Jiangsu Province, China;

<sup>2</sup> China University of Mining and Technology, Xuzhou 221116, Jiangsu Province, China;

<sup>3</sup> Hohai University, Nanjing 210024, Jiangsu Province, China.

\* Correspondence: ougeng@cumt.edu.cn

**Abstract:** Shield tunnel segments are prone to damage in practical use and require reinforcement. In order to test the reinforcement effect of internal adhesive steel plates on the segments, bending static tests were conducted on the standard block segments of shield tunnels. The effects of different burial depths (divided into mid buried segments and ultradeep buried segments) and different initial damage levels (initial loading values of 78% of the failure load of mid buried segments and 90% of the failure load of ultradeep buried segments) on reinforced shield tunnel segments strengthened by steel plates were studied. The changes in the main strain and displacement field of the reinforced shield tunnel standard block segments were measured using the digital image correlation (DIC) method, and the failure characteristics (including strain and crack development laws) of the reinforced shield tunnel were studied. The test results show that there is no significant change in the principal strain of the mid buried pipe segment in the early and middle stages of the bending static test after using internal adhesive steel plates for reinforcement. However, after using steel plates of the same size for reinforcement of the ultradeep buried pipe segment, many cracks and stress increases are evident in the early and middle stages of loading. In the later stage of loading, the strain of both types of reinforced segments at the end of the steel plate will suddenly increase, and the cracks will extend diagonally toward the midspan direction. When the final damage occurs, the steel plate falls off, and the end of the steel plate used to reinforce the pipe segment becomes a weak point. When the bending moment

changes from 500 kN to final failure, the displacement field of the buried pipe segment under initial loading to 78% of the failure load changes significantly, with the maximum value being 1.4 times the change in the ultradeep buried pipe segment under initial loading to 90% of the failure load. An internal adhesive steel plate can effectively improve the stiffness of the pipe segment and significantly reduce the displacement in both the X and Y directions of the pipe segment.

**Citation:** Li, X.; Geng, O.; Sun, Q. Study on the Mechanical Properties and Failure Characteristics of Reinforced Segments Based on DIC. *Prestress Technology* 2024, 2, 19-31. <https://doi.org/10.59238/j.pt.2024.02.002>

Received: 23/04/2024

Accepted: 25/06/2024

Published: 30/06/2024

**Keywords:** tunnel engineering; mechanical property; static bending test; shield tunnel segment; digital image correlation method

**Publisher's Note:** Prestress technology stays neutral with regard to jurisdictional claims in published maps and institutional affiliations.



**Copyright:** © 2024 by the authors. Submitted for possible open access publication under the terms and conditions of the Creative Commons Attribution (CC BY) license (<https://creativecommons.org/licenses/by/4.0/>).

## 1 Introduction

At present, shield tunneling is commonly used in the construction of subway tunnels in China. The shield tunneling method has the characteristics of high mechanization, guaranteed construction safety, and minimal impact on the surrounding area [1]. Prefabricated reinforced concrete segment structures are generally adopted for shield tunnel support [2]. However, due to initial design defects and engineering activities during service, many subway shield segments experience problems such as structural cracking and aging with increasing operating time [3]. Due to the large burial depth of the structure, it is difficult to replace the original structure. Scholars have proposed many reinforcement methods [4-6], and currently, secondary lining reinforcement methods are mostly used. The construction techniques of the pasting

steel plate reinforcement method [7] and the pasting carbon fiber cloth reinforcement method [8] are relatively simple and are widely used in engineering. Although the material selected for fiber cloth reinforcement is convenient, it has poor impermeability and insufficient stiffness to resist structural deformation. The addition of steel plates can improve structural stiffness, effectively control structural deformation, and result in good fire resistance and impermeability; thus, this approach has been widely used in engineering.

Kiriyama et al. [9] proposed the use of thin steel plates to reinforce tunnel segments to enhance their performance and demonstrated the feasibility of this method in practical engineering for the first time. Liu et al. [10] studied the ultimate bearing capacity of shield tunnels strengthened with full-scale internal tensioning steel rings and found that the stiffness and strength of the reinforced segments were significantly improved. Zhai et al. [11] established a model of steel plate reinforcement for shield tunnel segment circumferential seams, simulated the steel plate reinforcement of segment circumferential seams, and revealed the force transfer mechanism between the reinforcement steel plate and the segment. Liu et al., [12] established a three-dimensional solid finite element model on the basis of structural tests of shield tunnels strengthened with inner tensioned steel rings in an integral way [13,14]. By comparing the simulation and test data, they verified the consistency between the mechanical characteristics and the failure characteristics model of the tunnel lining strengthened with steel bonding and the actual test.

As a new non-contact and non-destructive optical measurement method, DIC has been widely used in recent years [15]. Unlike previous measurement methods, 3D-DIC technology can obtain full-range displacement and full-field strain results under loading with high resolution, reduced calibration time, and improved measurement results without causing errors.

This article adopts a full-scale standard block shield tunnel segment bonding steel plate reinforcement test, introduces digital image-related technology to achieve large-scale deformation measurements, analyzes the changes in the bending performance and failure characteristics of the segment, aims to explore the reinforcement effect of different steel plate specifications and reinforcement timing, quantitatively evaluates the effect of bonding steel plate reinforcement, and provides experimental support for subsequent theoretical research.

## 2 Digital Image Correlation (DIC)

The DIC method calculates sample deformation and displacement changes through speckle patterns on the surface of a specimen [16], which has the advantages of easy on-site operation, a wide measurement range, and the ability to obtain deformation in any direction. The measurement results are not affected by the shape or size of the measured object [17].

The basic principle is to compare geometric points on randomly distributed speckle images on the surface of the component and calculate the deformation of the component surface based on the motion changes of the points [18]. The specific approach is to first select a sample subarea in the image before deformation and select target points P and Q in this sample subarea, as shown in Figure 1. After the component undergoes deformation and displacement, the target subarea in the deformed image is searched for by calculating the peak value through the correlation function, and the corresponding displacement components  $u$  and  $v$  of the target points P' and

$Q'$  are calculated. The above calculation process is repeated to obtain the full-field displacement of the calculated area.

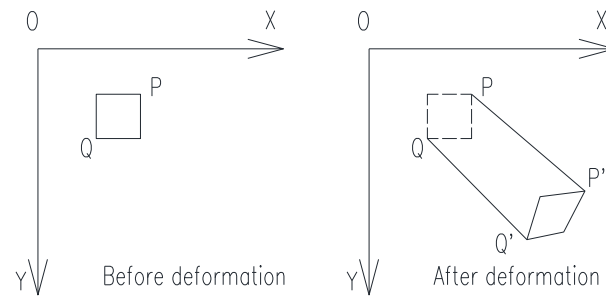


**Figure 1** Schematic diagram of subregions before and after deformation

The DIC test equipment included a loading system, light source, CCD camera, computing system, etc. The test process ensured the stability of the light source, sprayed matte paint on the surface of the test piece to artificially create speckle, adjusted the exposure and set the shooting frequency of the CCD camera after camera calibration, and then captured the distribution of speckle on the surface of the component and transferred it to the computer for image digitization, storing the grayscale information in the form of a matrix in the computer.

### 3 Experimental Design

#### 3.1 Design of Segment Specimens

The segment used in the Xuzhou Metro Project is adopted, with a concrete strength of C50, longitudinal reinforcement of HRB400, and stirrup of HPB300 grade steel. The reinforcement spacing is shown in Table 1. The reinforcement steel plate is a Q235B steel plate with a thickness of 10 mm. The thickness of the pipe segment is 350 mm, and the width is 1200 mm. Due to objective limitations such as experimental equipment, it is not possible to reinforce the segments under load. Instead, the method of loading and unloading can only be used to cause initial damage to the segments, and then the inner arc surface is pasted with steel plates. S1 and S2 were selected as reference specimens to determine the final bending load of the pipe segment. The principle for selecting the preload value is to use the maximum width of the surface crack of the pipe segment to reach 2 mm. The force control method is adopted, and the first vertical loading loads of pipe segments S3 and S4 are determined by referring to the maximum load values of the bending performance tests of S1 and S2. The conversion equation between the vertical load and mid-span bending moment is obtained through the balance equation. The initial loading bending moments of segments S3 and S4 are 392 kN·m and 497 kN·m, respectively, reaching 78% and 90% of the final loading values, as shown in Table 2.

**Table 1** Grouping of specimen design

Test piece number	Segment type	Outer curved surface longitudinal reinforcement	Inner curved longitudinal reinforcement	Stirrup
S1、S3	$10 < h \leq 16$	$10 \Phi 18$	$8 \Phi 20$	$14 \Phi 10$
S2、S4	$h > 22$	$2 \Phi 20 + 8 \Phi 22$	$8 \Phi 25$	$14 \Phi 10$

**Table 2** Segment design parameters

Test piece number	Upper soil cover thickness (m)	Reinforced or unreinforced	Final loading value (kN·m)	Preload value (kN·m)	Proportion of preload values
S1	Middle embedded depth	unreinforced	500	/	/
S2	Ultradeep embedded depth	unreinforced	553	/	/
S3	Middle embedded depth	reinforced	/	392	78%
S4	Ultradeep embedded depth	reinforced	/	497	90%

Each segment is equipped with four curved steel plates, with a size of 1,900 mm × 180 mm, with 5 holes evenly distributed on each steel plate, with a diameter of 10 mm. The size of the steel plate is shown in Figure 2, and the actual reinforcement of the plate is shown in Figure 3.

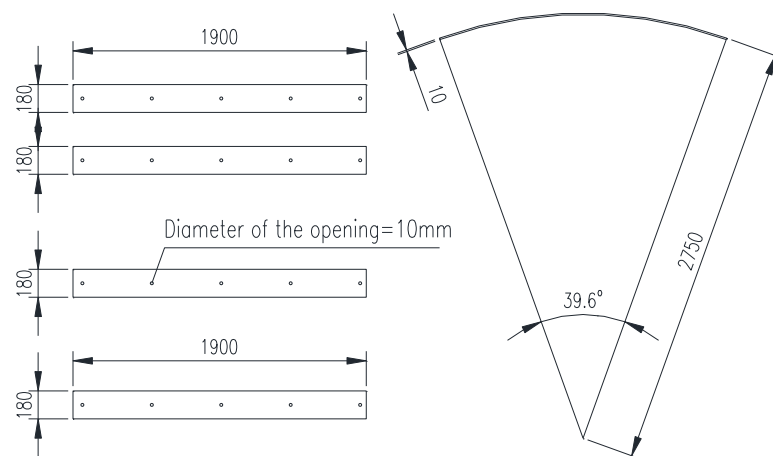


**Figure 2** Schematic diagram of the steel plate size (Unit: mm)



**Figure 3** Steel plate reinforcement diagram

### 3.2 Loading Device and Steps

The loading device consists of a reaction frame, a distribution beam, a hydraulic oil pump, a jack, a pressure sensor, and a sensor display device. In the bending performance test, the support at both ends of the pipe segment adopts a form like that of a simply supported beam: one end is horizontally constrained, and the other end can move horizontally. The self-designed all steel support is used as the base to support the specimen, consisting of three parts: the support part, the connection part, and the fixed part. A schematic diagram is shown in Figure 4, where 1 is a hollow support box structure welded with steel plates (20 mm thick), 2 is a hollow trapezoidal connection block composed of steel plates (20 mm thick), and 3 is a connecting anchor rod. According to CJJ/T 164—2011 "Technical Standards for Quality Inspection of Shield Tunnel Segments", the loading method adopts the two-point compression method, and the stress diagram and simplified diagram are shown in Figure 5. Considering the limitations of the experimental loading device, the loading method adopts the load control method. When the load is less than 900 kN, the increment of each level is 50 kN. When the load is greater than 900 kN, the increment is 25 kN, and the duration of each load level is 2-3 minutes. The loading pressure of the jack was manually controlled through the oil pump, and the specific load was read through the pressure indicator.

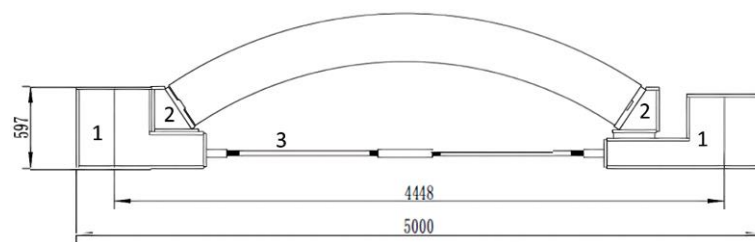


Figure 4 Schematic diagram of the segment and support (Unit: mm)

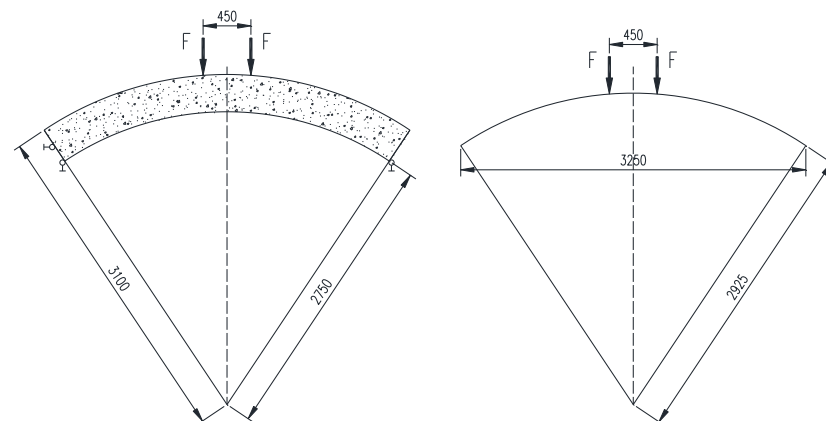


Figure 5 Segment force diagram (Unit: mm)

## 4 Analysis of Test Results

### 4.1 Changes in the Main Strain of the Pipe Segments

The entire testing process is monitored using 3D-DIC technology to obtain the propagation path of cracks in real time. In the later stage, the main strain of the sample surface is calculated using the GOM software analysis system, with a focus on analyzing images with typical changes. The side of the segment is taken as an example to analyze and discuss the results.

The failure process of the buried pipe segment S3, which was initially loaded to 78% of the failure load and then reinforced, is as follows.

When the bending moment  $M$  is small, there is no significant change in the principal strain diagram on the S3 side. As the bending moment increases, several evenly distributed vertical cracks appear in S3. When  $M=440 \text{ kN}\cdot\text{m}$ , as shown in Figure 6 a), the main strain at the end of the steel plate increases sharply, and cracks rapidly develop upward. The main strain suddenly changes locally at the end of the steel plate. When  $M$  increases from  $500 \text{ kN}\cdot\text{m}$  to final failure, as shown in Figure 6 b), the development of cracks can be clearly observed. The component is damaged from the end of the steel plate, and the concrete cracks and falls off.

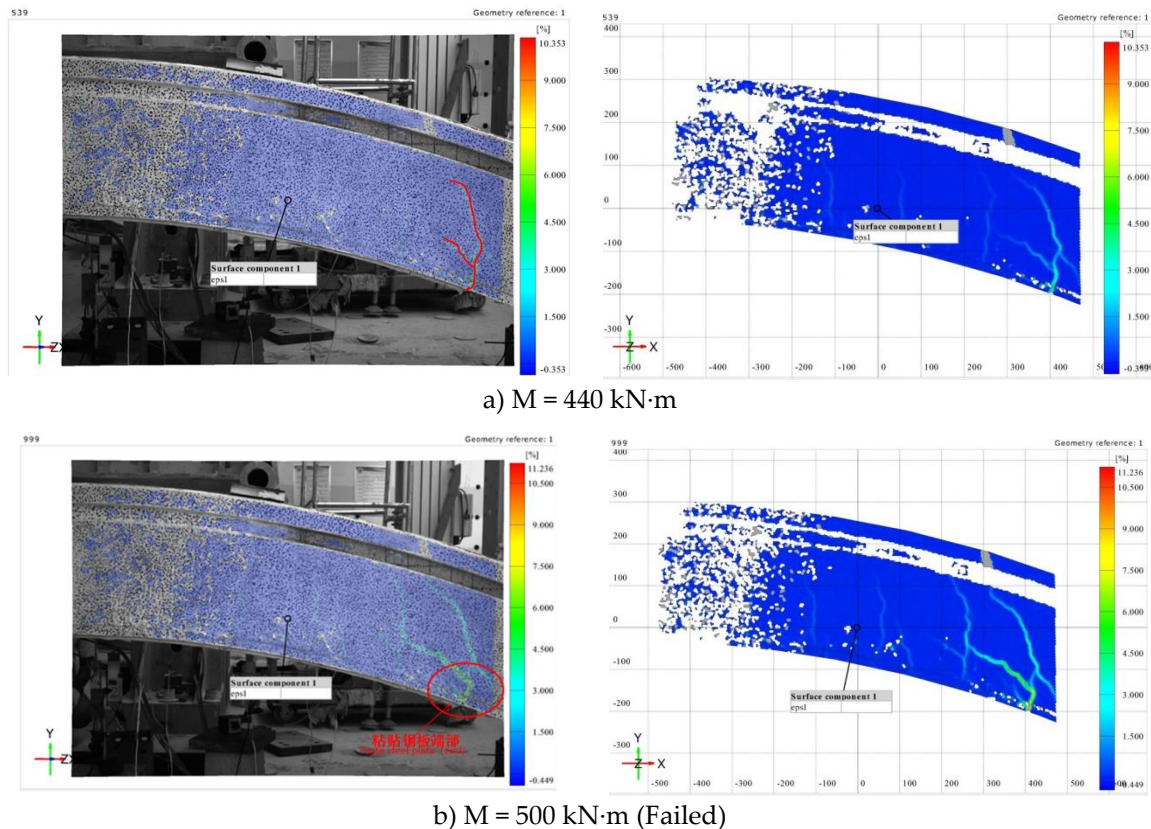
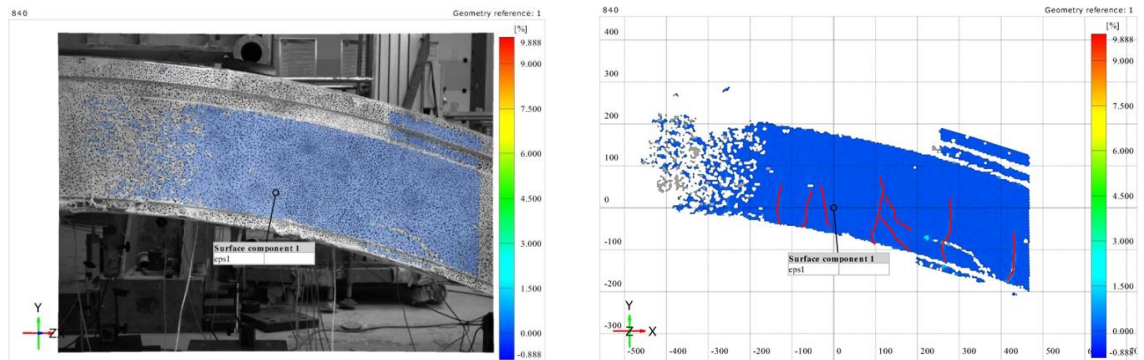


**Figure 6** Principal strain diagram of S3 under different loads

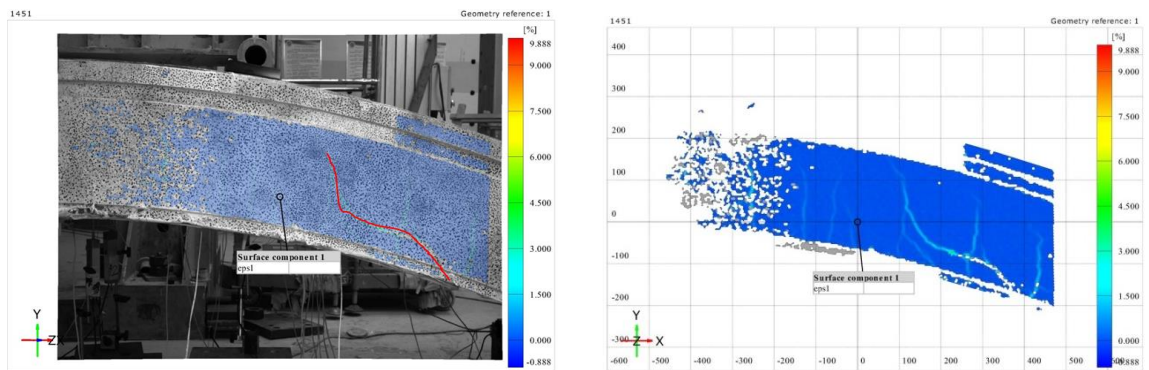
The failure process of the ultradeep buried segment S4 after initial loading to 90% of the failure load and reinforcement is as follows:

- (1) When  $M=265 \text{ kN}\cdot\text{m}$ , several linear cracks are distributed in the middle of the span, loading points, and ends, most of which are vertically upward, as shown by the red line in Figure 7 a).
- (2) When  $M=352 \text{ kN}\cdot\text{m}$ , the number of strain curves did not significantly increase, but the color of the curve deepened significantly, indicating an increase in strain.
- (3) When  $352 \text{ kN}\cdot\text{m} \leq M \leq 412 \text{ kN}\cdot\text{m}$ , the variation in S4 is more significant than that in S3, and there are multiple abrupt changes in the strain curve. Taking the typical three stages as an example, as shown in Figures 7 b) - d), the first stage is the sharp increase in cracks at the end of the steel plate, with a tendency to develop diagonally and horizontally toward the middle of the span. The second stage is the deepening of the curve color in the strain diagram and the obvious upward development of cracks. In the third stage, the line color on the strain diagram deepens and significantly widens, with the top extending to the height of the water stop channel and several small cracks extending around the main crack. Multiple small vertical and oblique cracks appear near the loading point and mid span.

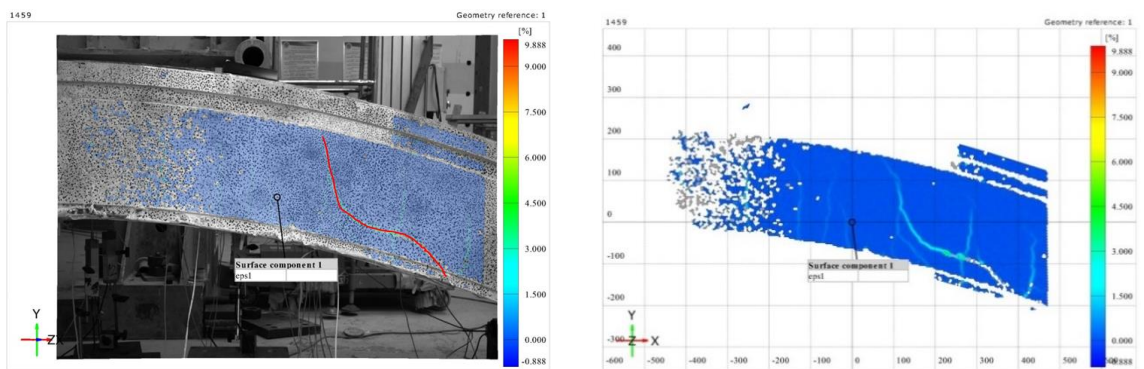
- (4) At the final failure, most of the cracks turn green, and some red segments appear at the lower end of the inclined cracks, with the curve becoming significantly thicker. The maximum strain occurs at the end of the steel plate near the lower side of the side.



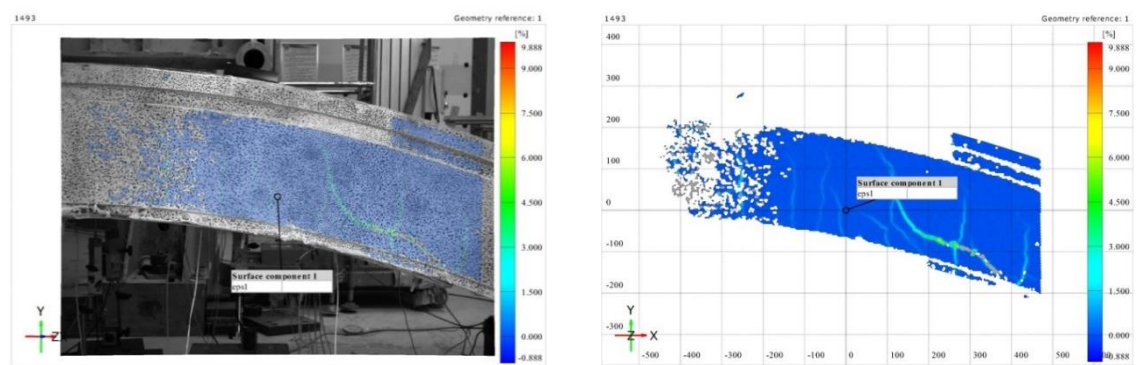
a)  $M = 265 \text{ kN}\cdot\text{m}$



b)  $352 \text{ kN}\cdot\text{m} \leq M \leq 412 \text{ kN}\cdot\text{m}$  (1st stage)

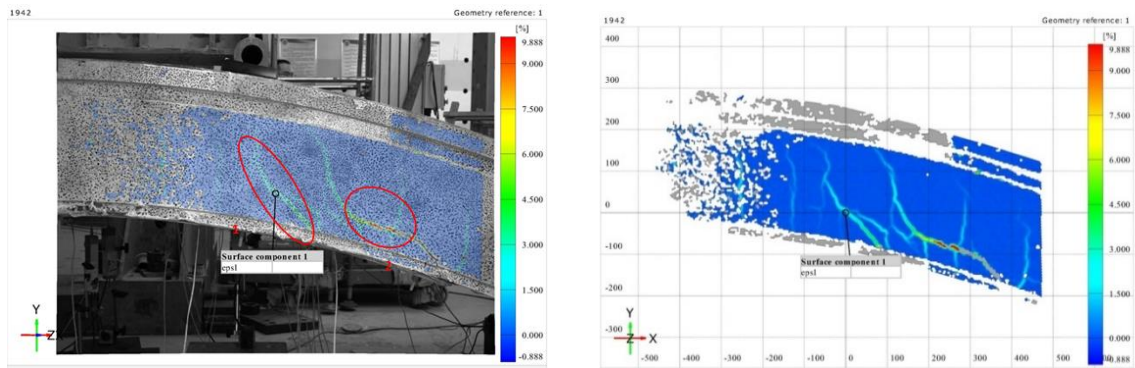


c)  $352 \text{ kN}\cdot\text{m} \leq M \leq 412 \text{ kN}\cdot\text{m}$  (2nd stage)



d)  $352 \text{ kN}\cdot\text{m} \leq M \leq 412 \text{ kN}\cdot\text{m}$  (3rd stage)

Figure 7 Continue



e) Final failure stage

**Figure 7** Principal strain diagram of S4 under different loads

According to the previous bending performance tests of S1 and S2, the maximum mid span bending moment of S1 is approximately 500 kN·m, and the maximum mid span bending moment of S2 is approximately 553 kN·m, indicating that the bearing capacity of S2 is better than that of S1. During the bending performance test of the reinforced pipe segment, there was no significant change in the main strain at the mid span, loading point, or outside the loading point of S3. Until failure, only the local damage at the end of the steel plate was severe, with fewer and finer cracks developing, and the damage range of the concrete was relatively small. Many cracks appeared and developed rapidly in the early and middle stages of S4 loading, and the location of the cracks was not limited to the end of the steel plate. The color change of the curve is obvious, indicating a significant increase in strain. The reason for this phenomenon may be that the initial damage of the segments is different. The performance of the mid buried segments after initial loading to 78% of the failure load is better than that of the ultradeep buried segments after initial loading to 90% of the failure load.

#### 4.2 Displacement Changes in the X-direction of the Segment

Unlike the local measurement points of the previous two horizontal displacement meters, 3D-DIC technology can calculate the displacement changes in the horizontal X direction on the side of the pipe segment, obtain the magnitude of the X direction displacement of 1/2 of the pipe segment and the displacement changes of the pipe segment, and also solve the problem of difficult placement of displacement meter monitoring points because the pipe segment is curved. In addition, the interface position of the pipe segment displacement changes in real time. Taking the key points of major strain mutation as the research object, the horizontal X-direction displacement changes in S3 and S4 after initial damage and reinforcement are analyzed.

Taking S3 as an example, in Figure 8 a) – c), the changes in the displacement field of S3 under different loads are shown, and in Figure 8 d), the changes in the displacement field during S3 failure are shown. From the figure, it can be clearly seen that the downward displacement field on the right side of the pipe segment has the largest change, followed by the middle and right sides of the pipe segment and finally the left side of the pipe segment, which is the mid span and outer curved surface of the pipe segment. The entire displacement change can be approximated as a fan shape that diffuses outward with the bottom right corner of the pipe segment as the center, with greater changes in the displacement field as it approaches the center.



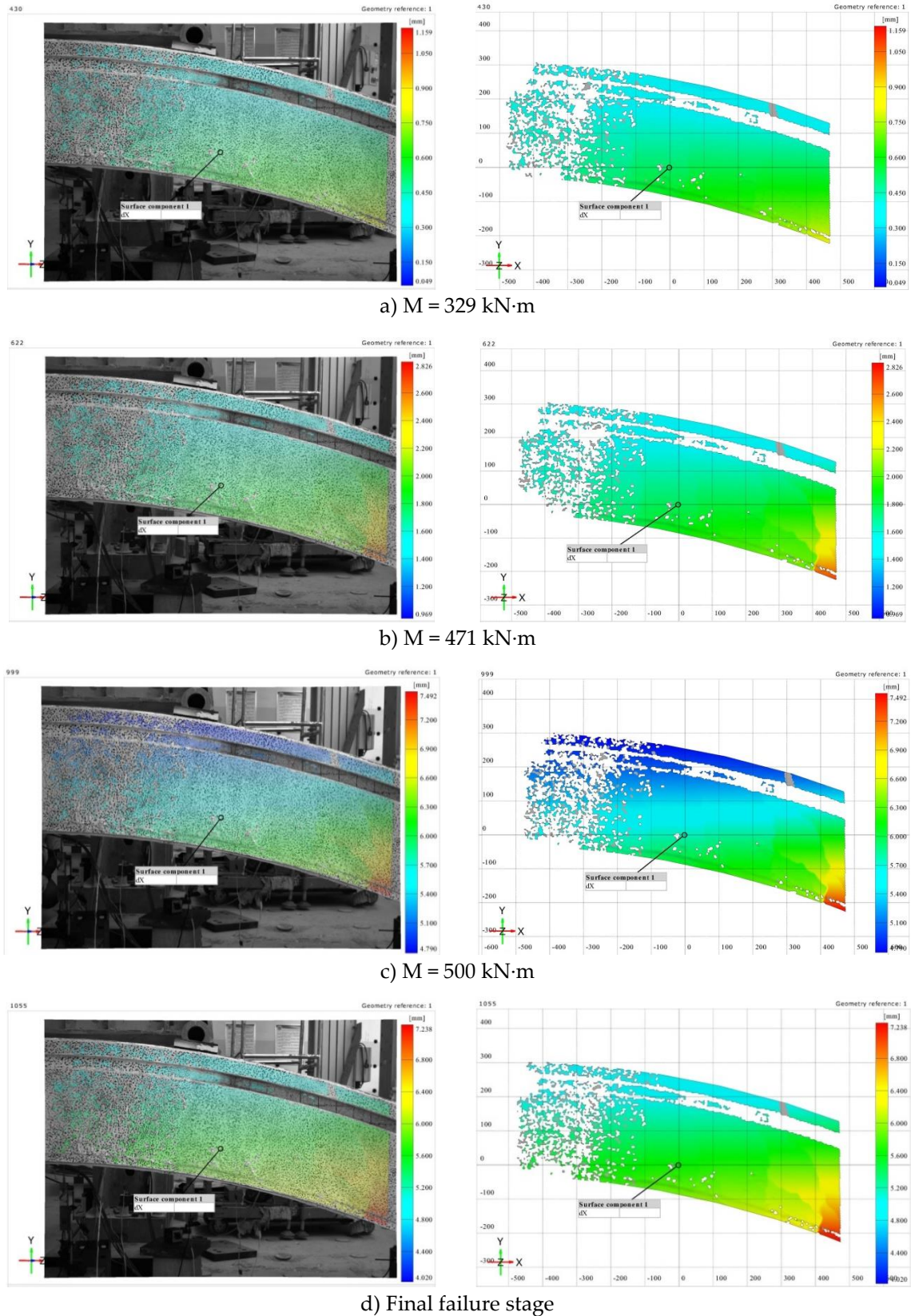


**Figure 8** Displacement field changes of S3 in the X direction under different loads

By comparing and analyzing the changes in the displacement field of segments S3 and S4, it can be concluded as follow.

The final failure modes of S3 and S4 are similar, both of which are caused by the peeling of the end of the bonded steel plate, resulting in a sharp increase in pipe cracks and the peeling of concrete blocks.

- (1) When  $M=179 \text{ kN}\cdot\text{m}$ , Figure 9 shows that the displacement change in S3 is very small, not exceeding 0.3 mm, while the displacement change in S4 ranges from 0.5 mm to 1 mm.
- (2) When  $329 \text{ kN}\cdot\text{m} \leq M \leq 359 \text{ kN}\cdot\text{m}$ , the increase in S3 is not significant, while the increase in S4 is relatively large, with a maximum value of approximately 3.25 mm, which is approximately four times the maximum value of S3.
- (3) When  $419 \text{ kN}\cdot\text{m} \leq M \leq 471 \text{ kN}\cdot\text{m}$ , the growth rates of S3 and S4 are significantly accelerated, and the growth rate of S4 is much faster than that of S3. The maximum displacement change of S4 is as high as 6 mm, and the minimum value is approximately 3.75 mm. The maximum displacement change of S3 is approximately 2.5 mm, which is similar to the minimum displacement change of S4 in the middle stage of loading. It can be observed that pasting steel plates has a better reinforcement effect on buried pipe segments.
- (4) When  $M$  changes from  $500 \text{ kN}\cdot\text{m}$  to final failure, as shown in Figure 10, the change in the displacement field value of S4 is not significant. S3 undergoes a sudden change, and the change value increases by approximately 3 times, with a minimum value of 5 mm, which exceeds the minimum displacement value of S4. The change in S3 is as high as 8 mm, which is approximately 1.4 times that of S4. The reason for this reversal may be that after the steel plate falls off, the pipe segment loses its reinforcement effect and is in an unreinforced state. The bearing capacity of the ultradeep buried pipe segment is better than that of the medium buried pipe segment, which is consistent with the results of the early S1 and S2 bending performance tests.

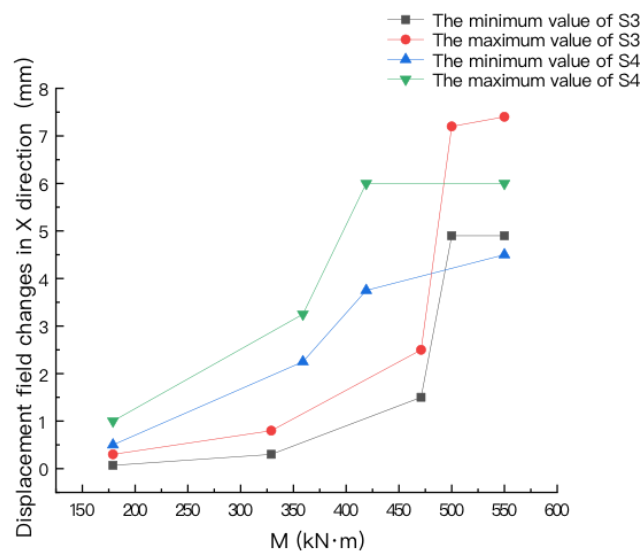


Figure 9 Displacement field changes in the X direction for S3 and S4

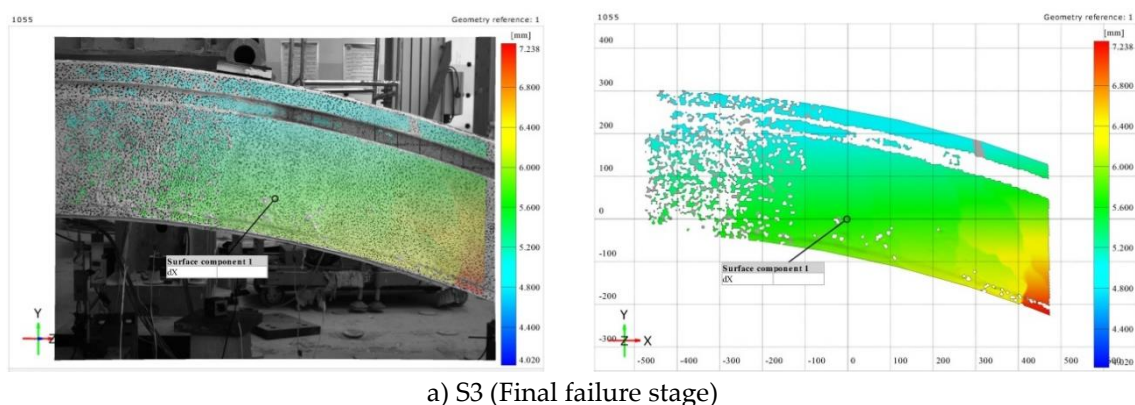
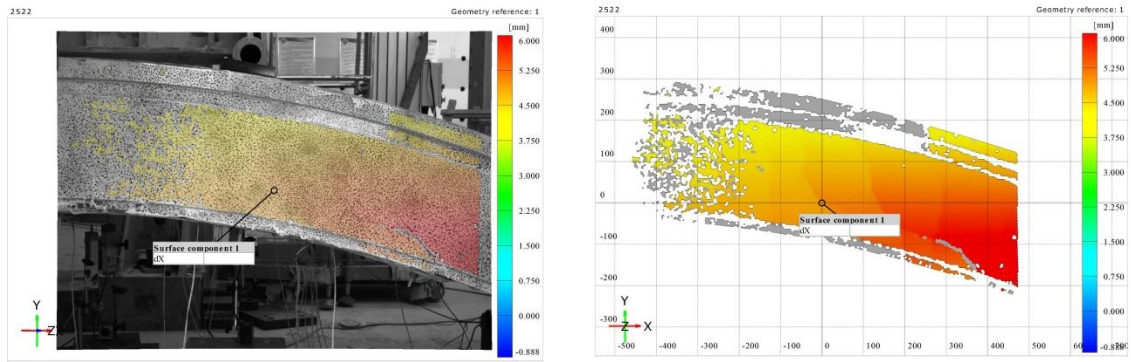


Figure 10 Continue



b) S4 (Final failure stage)

**Figure 10** Displacement field changes in the X direction when S3 and S4 are damaged

### 4.3 Changes in the Y-direction Displacement of the pipe segments

For the segment, the displacement in the Y direction is also important. By using 3D-DIC, the displacement change in the horizontal Y direction of the segment sample surface can be obtained. Taking the buried segment S3 as an example, comparing the displacement field changes in the X and Y directions, as shown in Figure 11, the analysis shows the following:

The variation pattern of the horizontal displacement in the Y direction in S3 is similar to that in the X direction, both decreasing from the mid span to the right end, and the growth pattern is also similar. In the early and middle stages of loading, the growth rates of the displacement field change in both directions are similar, with the Y direction slightly greater than the X direction. However, when  $M=500 \text{ kN}\cdot\text{m}$ , there is a wave peak in the displacement field in the X direction, indicating that pasting steel plates can effectively enhance the stiffness of the damaged pipe segments in both directions, and the reinforcement effect is not significantly different. The reason for the wave peak in the X direction may be that when  $M=500 \text{ kN}\cdot\text{m}$ , the reinforced pipe segments reach the maximum bearing capacity limit in the X direction, which is consistent with the maximum load value in the S1 bending performance test.

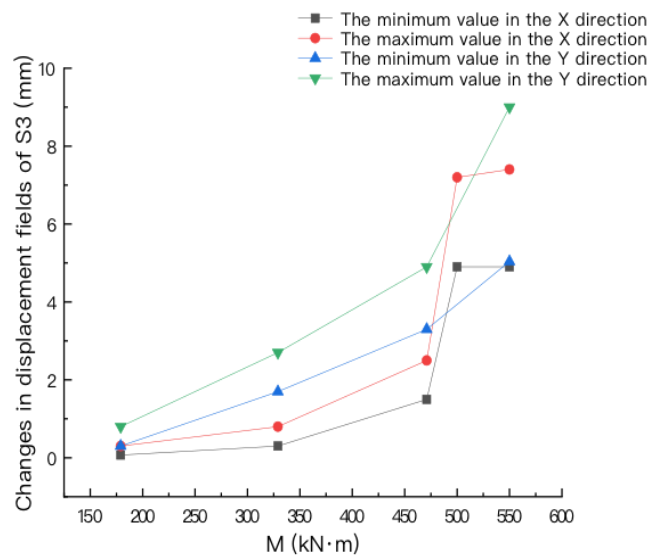


**Figure 11** Changes in displacement fields in the X- and Y-directions of S3

## 5 Conclusions

Based on 3D-DIC technology, the 1/2 side of the pipe segment was selected as the observation sample surface to observe the entire process of the bending static test of the reinforced pipe segments with different burial depths. The changes in the

displacement field in the X- and Y-directions were compared and analyzed, and a principal strain analysis was conducted. The load values corresponding to the sudden change points, or the range of graded loads were found, and the strain and crack development on the side of the pipe segment were obtained. The conclusions are as follows.

- (1) After using steel sheets of the same specification for reinforcement, due to different initial loading values, the strain changes in the two types of pipes in the early and middle stages of loading are different. The medium buried pipes that were first loaded to 78% of the failure load showed no significant strain changes in the early and middle stages of loading, while the ultradeep buried pipes that were first loaded to 90% of the failure load showed many obvious cracks at  $M=265 \text{ kN}\cdot\text{m}$ . In the middle stage of loading, the development of cracks became more obvious, and the number of cracks increased sharply.
- (2) In the later stage of loading, the strain of both types of pipe segments at the end of the steel plate increases sharply, and the cracks develop rapidly diagonally toward the midspan until ultimate failure. Therefore, when using adhesive steel plate reinforcement in practical engineering, the end of the steel plate should be considered a danger point, and the position of the end of the steel plate should be reasonably arranged.
- (3) In the early and middle stages of loading, the displacement change in the middle-buried pipe segment is very small, while the displacement changes in the ultradeep buried pipe segment increases significantly. The maximum displacement change is approximately 2.4 times the maximum value of the middle-buried pipe segment, indicating that the addition of steel plates for reinforcement is effective for the middle-buried pipe segment.
- (4) By comparing the load-bearing capacity of the bending resistance performance, it can be observed that steel plate reinforcement can improve the stiffness of the tunnel segment to a certain extent and play a significant role in controlling the horizontal displacement of the shield tunnel segment in both directions. A reasonable design can ensure that the reinforced segment can reach a load-bearing capacity similar to that of the original segment even if initial damage occurred.
- (5) When the steel plate specifications and test environment are consistent, there is a reversal phenomenon in the later stage of the bending performance test of the pipe segment. When not reinforced, the maximum load of the bending performance test of the ultradeep buried pipe segment is slightly greater than that of the medium buried pipe segment, while the performance of the reinforced ultradeep buried pipe segment after initial loading to 90% of the failure load is actually lower than that of the medium buried pipe segment after initial loading to 78% of the failure load, possibly due to different initial damage conditions of the pipe segment. This point can be further studied in the future.

**Conflict of Interest:** All authors disclosed no relevant relationships.




**Date Availability Statement:** The data that support the findings of this study are available from the corresponding author, Geng, upon reasonable request.

## References

1. Liu, X.; Zhang, J.; Jiang, Z.; Liu, Z.; Xu, P.; Li, F. Experimental Investigations of a Segmental Tunnel Ring Strengthened by Using UHPC. *China Journal of Highway and Transport* **2021**, *34*, 181-190, doi:10.19721/j.cnki.1001-7372.2021.08.015.
2. Li, J.; Lei, M.; Lin, Y.; Dai, X.; Liu, T. Causes Analysis and Safety Evaluation of Cracking Shield Segment. *Journal of Railway Science and Engineering* **2018**, *15*, 1786-1792, doi:10.19713/j.cnki.43-1423/u.2018.07.021.

3. Zhu, W.; Ju, S. Causes and Countermeasures for Segment Cracking in Shield- Driven Tunnel. *Modern Tunnelling Technology* **2003**, 21-25, doi:10.13807/j.cnki.mtt.2003.01.005.
4. Wu, B.; Luo, Y.; Zang, J. Experimental Study on Mechanical Performance of Tunnel Segment Joints Strengthened Using Concrete-Filled Steel Tubes. *Journal of Building Structures* **2019**, 40, 105-112, doi:10.14006/j.zjgxb.2017.0775.
5. Liu, X.; Jiang, Z.; Liu, S. Experiment of Deformed Shield Tunnels Strengthened by Steel Plate-concrete Composite Structure. *China Journal of Highway and Transport* **2020**, 33, 128-137, doi:10.19721/j.cnki.1001-7372.2020.01.013.
6. Chen, R.; Lu, L.; Zhang, Y.; Wu, H. Reinforced Technology and Mechanical Properties of Shield Tunnel Lining with UHPC. *Engineering Mechanics* **2019**, 36, 41-49, doi:10.6052/j.issn.1000-4750.2018.11.0620.
7. Piekarczyk, M.; Grec, R. Application of Adhesive Bonding in Steel and Aluminium Structures. *Archives of Civil Engineering* **2012**, 58, 309-329.
8. Zhou, D. Calculation Method of CFRP Strengthened Highway Tunnel Lining Based on Reliability Theories. Master, Tongji University, Shanghai, 2008.
9. Kiriya, K.; Kakizaki, M.; Takabayashi, T.; Hirosawa, N.; Imafuku, K. Structure and Construction Examples of Tunnel Reinforcement Method Using Thin Steel Panels. *Nippon Steel Technical Report* **2005**, 45-50.
10. Liu, X.; Zhang, H.; Tang, M.; Lu, L.; Wang, X. Experimental Study of the Ultimate Bearing Capacity of a Shield Tunnel Reinforced by a Semi-Ring Steel Plate. *Modern Tunnelling Technology* **2014**, 51, 131-137, doi:10.13807/j.cnki.mtt.2014.03.021.
11. Zhai, W.; Zhai, Y.; Zhang, D.; Wu, H.; Huang, H. Numerical Study on Shearing Performance of Steel Plate Strengthened Circumferential Joints of Segmental Tunnel Linings. *Chinese Journal of Geotechnical Engineering* **2019**, 41, 235-239, doi:10.11779/CJGE2019S2059.
12. Liu, T.; Huang, H.; Xu, R.; Yang, X. Research on Load-bearing Capacity of Metro Shield Tunnel Lining Strengthened by Bonded Steel Plates. *China Journal of Highway and Transport* **2017**, 30, 91-99, doi:10.19721/j.cnki.1001-7372.2017.08.010.
13. Liu, X.; Tang, M.; Lu, L.; Wang, X.; Zhu, Y. Experimental Study of Ultimate Bearing Capacity of Shield Tunnel Reinforced by Full-Ring Steel Plate. *Chinese Journal of Rock Mechanics and Engineering* **2013**, 32, 2300-2306.
14. Bi, X.; Liu, X.; Wang, X.; Lu, L.; Zhu, Y. Experimental Study on the Ultimate Load-Bearing Capacity of Deformed Segmental Tunnel Linings Strengthened by Steel Plates. *China Civil Engineering Journal* **2014**, 47, 128-137, doi:10.15951/j.tmgxcb.2014.11.048.
15. Dai, S.; Ma, S.; Pan, Y.; Dong, Z. Evaluation of Mode I Stress Intensity Factor of Rock Utilizing Digital Speckle Correlation Method. *Chinese Journal of Rock Mechanics and Engineering* **2012**, 31, 2501-2507, doi:10.3969/j.issn.1000-6915.2012.12.014.
16. Zhang, D. Digital Image Correlation: Theory and Applications. *Journal of Medical Biomechanics* **2009**, 24, 85-88+93.
17. Chen, F.X.; Chen, X.; Xie, X.; Feng, X.; Yang, L.X. Full-Field 3D Measurement Using Multi-Camera Digital Image Correlation System. *Opt Laser Eng* **2013**, 51, 1044-1052, doi:10.1016/j.optlaseng.2013.03.001.
18. Zhao, Y.; Xing, Y.; Huang, J.; Jiang, A. Study on the Fiber-Reinforced Concrete Pull-Out Test Using Digital Image Correlation Method. *Engineering Mechanics* **2010**, 27, 169-175.

AUTHOR BIOGRAPHIES

	<p><b>Xiao Li</b> M.E, Senior Engineer, Working at China Railway Shanghai Design Institute Group Co., Ltd. Research Direction: Tunnel structure design and reinforcement. Email: lixiao@sty.sh.cn</p>		<p><b>Ou Geng</b> D.Eng. Professor, Working at China University of Mining and Technology. Research Direction: Durability of concrete structures. Email: ougeng@cumt.edu.cn</p>
	<p><b>Qian Sun</b> Doctoral students in progress, Studying at Hohai University. Research Direction: Engineering Structural Design and Numerical Simulation.</p>		